Computer Aided Geometric Design 43 (2016) 226–236

Contents lists available at ScienceDirect

Computer Aided Geometric Design

www.elsevier.com/locate/cagd

Make it swing: Fabricating personalized roly-poly toys

Haiming Zhao [a], Chengkuan Hong [b], Juncong Lin [c,*], Xiaogang Jin [a], Weiwei Xu [a]

[a] State Key Lab of CAD&CG, Zhejiang University, Hangzhou 310058, China
[b] School of Mathematical Sciences, Zhejiang University, Hangzhou 310058, China
[c] Software School of Xiamen University, Xiamen 361005, China

ARTICLE INFO

Article history:
Available online 27 February 2016

Keywords:
Roly-poly toys
Dynamic equilibrium
Computer aided design
3D printing

ABSTRACT

A roly-poly toy is considered as one of the oldest toys in history. People, both young and old, are fascinated by its unique ability to right itself when pushed over. There exist different kinds of roly-poly toys with various shapes. Most of them share a similar bottom which is a hollow hemisphere with a weight inside. However, it is not an easy task to make an arbitrary model to swing like a roly-poly due to the delicate equilibrium condition between the center of mass of the roly-poly toy and the shape of the hemisphere. In this paper, we present a computer-aided method to help casual users design a personalized roly-poly toy and fabricate it through 3D printing with reduced material usage and sufficient stability. The effectiveness of our method is validated on various models. Our method provides a novel easy-to-use means to design an arbitrary roly-poly toy with an ordinary 3D printing machine, extricating amateurs from the dilemma of finding extra weight to balance the shape.

1. Introduction

A roly-poly toy, which is also referred to as a tumbler, is usually a round-bottomed doll. It is considered as one of the oldest toys in history. The bottom of a traditional roly-poly toy is roughly a hemisphere, so that it is able to right itself when pushed over. Over the years, different-looking roly-poly toys are produced across the world, such as animals, clowns, and celebrities. They have come to symbolize the ability to have success, overcome adversity, and recover from misfortune (Kyburz, 1994).

Traditional roly-poly toys usually consist of two parts (Wikipedia, 2016). The upper part has an amazing variety of shapes influenced by culture and manufacturers. The lower part (base part) is mostly round and roughly a hemisphere, which is generally hollow with a metal weight inside to balance the center of mass. The shape of the lower part and the center of mass of a roly-poly toy are carefully designed for regaining balance by itself. However, creating a personalized roly-poly toy is traditionally a cut-and-try process which requires moderate attempts and experiences. A key problem is to keep a delicate equilibrium between the center of mass of the toy and the shape of the lower part. Usually, a carefully selected metal weight is located in the base (vigothecarpathian, 2015; krokotak.com, 2015).

3D printing enables everybody to easily fabricate 3D models. However, making a personalized roly-poly toy is still a nontrivial process for ordinary users as the input mesh must be edited carefully to keep the equilibrium. Moreover, most 3D printers use the same material which makes it even harder to balance the roly-poly toy and make it swing.

* Corresponding author.
E-mail address: jclin@xmu.edu.cn (J. Lin).

http://dx.doi.org/10.1016/j.cagd.2016.02.001
0167-8396/

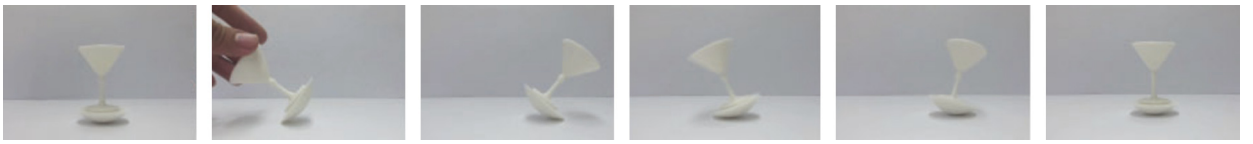

Fig. 1. A goblet shape roly-poly toy example designed by our method. The snapshots show that the toy is able to regain balance when pushed over.

Much attention has been devoted in the field of fabricating models with certain structures associated with static equilibrium and motion. Prévost et al. (2013) aimed to fabricate static models that stand in various poses. Bächer et al. (2014) took a step further to spin it. Different from previous work, in our case, the toy to be printed should balance on the initial standing position and restore to the balancing state after being pushed over or rotated. Therefore, our design will result in different equilibrium conditions and constraints for optimization in order to account for the special dynamic properties of roly-poly toys. When designing the equilibrium constraint, we should take the shape of toy, the stability of restoring balance, and the swing amplitude into consideration.

In this paper, we present a novel framework to help amateurs design personalized roly-poly toys. (See Fig. 1.) In our interactive design system, the upper part mesh of a roly-poly toy is provided by users. The input mesh is firstly optimized in terms of mass distribution. Then, a corresponding base part is calculated. Finally, the generated results are fabricated through 3D printing. Besides the reduced material usage constraint, our approach can maintain sufficient stability and attain amplitude of swing as large as possible. We have conducted extensive experiments on a variety of models to validate our pipeline, which are demonstrated in the accompanying video.

The contributions of this paper lie in the following main aspects: (i) We present a novel framework to fabricate roly-poly toys which can theoretically guarantee the stability of the printed toy. To the best of our knowledge, this is the first approach to design personalized roly-poly toys through 3D printing. (ii) We formulate the design process as an optimization problem so as to reduce the printing material and maintain dynamic characteristics of the resulting toy. (iii) We develop a method to print the whole toy with the same material without using traditional metal weight to balance the center of mass.

2. Related work

3D Printing stimulates a significant amount of research interests in the computer graphics community recently. With the help of simulation techniques, some methods have been developed to optimize 3D shapes to satisfy specific elastic deformation constraints under external forces (Bickel et al., 2010; Chen et al., 2014). Shape optimizations are introduced to reduce supporting structures and speed up the printing process (Kwok et al., 2015; Zhang et al., 2015; Hu et al., 2015). Adding 3D-printable joints provides a solution to produce functional posable models (Bächer et al., 2012; Calì et al., 2012). Mechanical motion is achieved using mechanical automata (Coros et al., 2013; Ceylan et al., 2013). Offset surfaces can also be employed to reduce printing materials by making printed objects hollow (Liu and Wang, 2011; Wang and Manocha, 2013). To optimize the mass distribution and the stability of printed objects, Musialski et al. (2015) proposed a reduced-order shape optimization method by using offset surfaces with varying thickness. In addition, surfaces with desired spatially varying reflectance can be fabricated (Lan et al., 2013; Chen et al., 2013). Different from previous methods, we provide an insight into fabrication-oriented design towards dynamic equilibrium.

Structural stability analysis under varied loading conditions plays a crucial role in printing digital models. It helps to detect the weak regions and enhance its printability through the shape optimization. Whiting et al. (2009, 2012) introduced the idea of generating structurally feasible models of buildings. They used the measure of infeasibility as an energy function and optimized the energy to satisfy structural constraints. Panozzo et al. (2013) designed unreinforced masonry models. Deuss et al. (2014) applied and extended the framework to successfully assemble self-supporting structures. To satisfy the stress constraints, Stava et al. (2012) added support structure and adjusted the thickness of the surface mesh. Zhou et al. (2013) proposed an easy-to-use framework to analyze the worst load distribution by means of a fast linear element-based method. Besides improving structural stability, we also focus on adjusting the center of mass using shape optimization.

The delicate balance between static equilibrium and dynamic motion is fascinating. The approach proposed by Prévost et al. (2013) drew researchers' attention to fabricate static models that stand in various poses without requiring glue or pedestals. Bächer et al. (2014) took a step further in dynamic equilibrium. They proposed an impressive framework to optimize the rotational stability using a combination of hollowing inside, cage-based deformation, and dual-material models. Different from them, we are interested in solving the static and dynamic equilibrium of a roly-poly toy. The process formulation, variables, and constraints involved are quite different from previous methods.

Toy design. Researchers have devoted much to the delightful design process of toy manufacturers (Mitani and Suzuki, 2004; Igarashi and Igarashi, 2009; Zhu et al., 2012; Guo et al., 2014). Puzzles with interlocking pieces are fabricated (Lo et al., 2009; Xin et al., 2011; Song et al., 2012). Mori and Igarashi (2007) introduced an interactive system to conveniently design personalized plush toys. Based on sketch interface, this system facilitates various editing operations tailored for plush toy design. Later on, 3D printing becomes an active part in toy design, especially for toys with sophisticated geometry characteristics. Hirose et al. (2011) proposed an interactive system to design the unique solid "sphericon" with additional conditions like geometric and symmetry constraints. Mueller et al. (2014) presented a layout refinement algorithm that

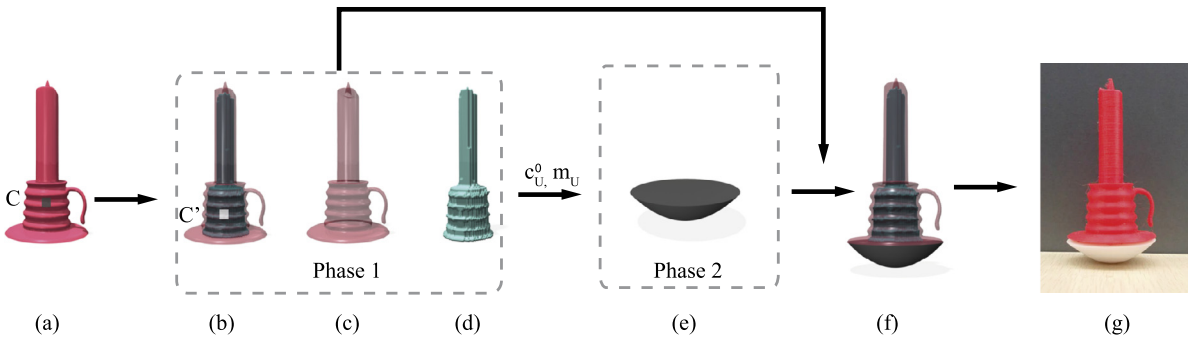

Fig. 2. System overview of our approach. Given a 3D shape as input mesh (a), we first optimize the upper part $\mathcal{U}$ of the roly-poly toy in Phase 1. (a) is hollowed as shown in (b). The outer surface and the inner surface are shown in (c) and (d). After the optimization in Phase 1, the position of center of mass for $\mathcal{U}$, as c_U^0 in Equation (10) and the mass of $\mathcal{U}$, as m_U in Equation (22) are determined and set as initial value for Phase 2. The parameters a, r for $\mathcal{L}$ are optimized in Phase 2 (e). Thus, an optimized result is generated (f). $\mathcal{U}$ and $\mathcal{L}$ are printed separately and then glued together to generate the final roly-poly toy (g).

iteratively improved the structure. Luo et al. (2015) presented a new approach to rapid prototyping functional objects using bricks-like LEGO bricks. Different from them, we focus on designing personalized roly-poly toys.

Torque and energy in rotational motion. The torque acting on the particle is proportional to its angular acceleration (Halliday et al., 1992), which is useful in describing the self-righting motion of roly-poly toys when pushed over. The energy concept of converting between kinetic energy and potential energy can be equally useful in understanding rotational motion. A well-designed roly-poly toy requires center of mass (Eberly, 2010) and the shape of the base part of the roly-poly toy to satisfy specified constraint. To fabricate personalized roly-poly toys, we formulate the above-mentioned constraints into an optimization process. The self-righting property of a roly-poly toy inspires researchers to design input devices for 3D interaction. Based on the hemispherical shape and free moving property of the roly-poly toy, Perelman et al. (2015) designed a roly-poly mouse to unify 2D and 3D interactions, which managed to create compound gestures such as translation, roll, and rotation.

3. Method overview

A roly-poly toy ($\mathcal{M}$) usually consists of a lower part ($\mathcal{L}$) and an upper part ($\mathcal{U}$). The shape of $\mathcal{U}$ is usually carefully designed to attract people. $\mathcal{L}$ has a hemisphere-like shape and plays a key role in balancing the toy. We assume that the shape of $\mathcal{L}$ is a paraboloid of revolution. Based on these observations, we divide our framework into two phases: Phase 1 is used to optimize the upper part $\mathcal{U}$ by adjusting its material distribution and its position on $\mathcal{L}$; Phase 2 is employed to optimize the coefficient a, which dictates the level of curvature for the paraboloid of revolution, and radius r of the lower part $\mathcal{L}$. Once the users specify some necessary parameters, such as printing material and dimension, the system will automatically compute $\mathcal{U}$ and $\mathcal{L}$. We finally combine the two parts by gluing $\mathcal{U}$ on top of $\mathcal{L}$ to get the final personalized roly-poly toy. In the following sections, we will describe each optimization process in detail.

3.1. Computational model

Fig. 3 is a discrete illustration of our roly-poly model. An input mesh is taken as $\mathcal{U}$ of a roly-poly toy. A minimal wall thickness is set to meet the basic standard for 3D printing fabrication. The inner and outer surface meshes are represented as M_I and M_O, respectively.

In our framework, the shape of $\mathcal{L}$ is a paraboloid. The reason for using a paraboloid is that it can represent more shapes than circular arcs by adjusting the level of curvature. Therefore, $\mathcal{L}$ can be described by the following function:

$$z = ax^2 + ay^2, \tag{1}$$

where a is a coefficient to dictate the level of curvature of the paraboloid of revolution.

The standing position of the roly-poly toy is set as the initially balanced position (shown in Fig. 3(a)). Thus, the center of mass C for the roly-poly toy should lie on the middle axis. As it is pushed away from the initial position, the contact point on the supporting plane switches from O to A (see Fig. 3(b)). For simplicity, we set the origin of the coordinate as O and assume the Z direction is along the middle axis of the roly-poly toy. The blue line indicates the supporting plane and B is the intersection of the Z axis and the gravity direction. We project paraboloid of revolution on X–Z plane, the projected curve is a parabola equation:

$$z = ax^2, \tag{2}$$

where a is the same coefficient used in Equation (1), which equals to the reciprocal of the latus rectum for this parabola.

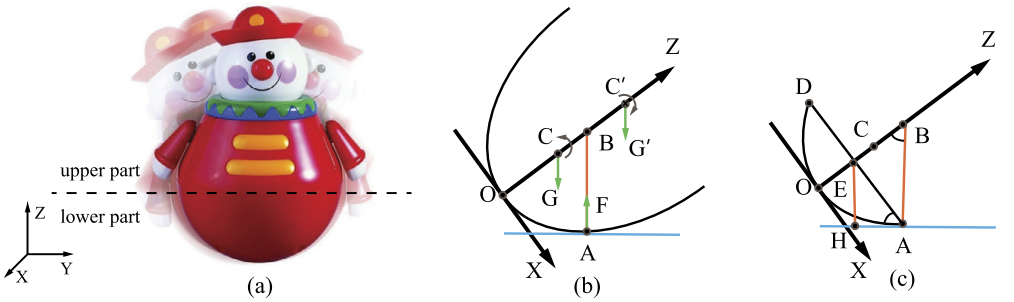

Fig. 3. The requirement for the center of mass. (a) shows a roly-poly chiming clown. (b) and (c) are viewed along Y axis. (b) is a simple illustration for calculating the best location for center of mass for the roly-poly toy. The amplitude of swing is calculated in (c). $OAED$ denotes the optimized $\mathcal{L}$ and the angle ABC indicates upper limit of balancing by itself.

3.1.1. Center of mass

Let m be the mass of the roly-poly toy shown in Fig. 3(a). We use dm to represent the mass at point $P = (x, y, z)$. Then the center of mass (x_c, y_c, z_c) of the toy can be simply calculated by Halliday et al. (1992), Eberly (2010):

$$x_c = \frac{1}{m}\int x dm,\ y_c = \frac{1}{m}\int y dm,\ z_c = \frac{1}{m}\int z dm. \tag{3}$$

3.1.2. Equilibrium condition

Righting itself when pushed over is one of the main characteristics of a roly-poly toy. We assume that a roly-poly is put on the table with its standing position as the balancing position. At the moment the roly-poly toy is pushed over, it gains an initial kinetic energy. When the roly-poly toy swings away from the balancing position, its kinetic energy is transformed into potential energy and the speed of the swing decreases. Afterwards, the potential energy is transformed back into kinetic energy which reaches the maximal at the balancing position. Because of the friction of the table and the air, the roly-poly toy is able to reach its balance at the initial position when its center of mass meets some requirements. Fig. 3(b) illustrates the situation when Fig. 3(a) is pushed over to the right. A is the contact point for $\mathcal{L}$, which is drawn as the parabola curve. B is the intersection point of direction of supporting force F and the Z axis. Let the coordinate of center of mass C for the roly-poly toy be $(0, c)$. Considering the torque (Halliday et al., 1992) associated with the gravity with the wrench pivoted on the axis through A, the direction of this torque determines the rotation of the roly-poly toy. If C is lower than B in Z direction, the roly-poly toy tends to swing back to the balancing position. If the center of mass is located on C', under the influence of torque derived by gravity, the roly-poly tends to fall.

The constraint for C is calculated as follows. The slope for point $A = (x_0, z_0)$ on the curve is:

$$k = 2ax_0. \tag{4}$$

The equation for the line AB can be described as:

$$z - z_0 = -\frac{1}{2ax_0}(x - x_0), \tag{5}$$

which can be rewritten as:

$$z = -\frac{1}{2ax_0}x + \frac{1}{2a} + ax_0{}^2. \tag{6}$$

Thus the coordinate of B is $(0, \frac{1}{2a} + ax_0{}^2)$. The roly-poly toy will restore its balance as long as the following condition is satisfied:

$$c < \frac{1}{2a} + ax_0{}^2. \tag{7}$$

Therefore, the center of mass C should satisfy the following equation with any contact point A on the curve:

$$0 \le c \le \frac{1}{2a}. \tag{8}$$

Considering the coordinate system we adopted in Section 3.1, the center of mass can be calculated separately according to x, y, z coordinates.

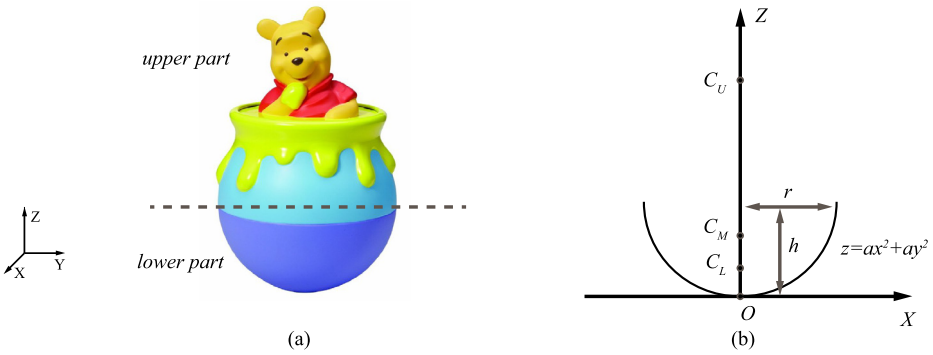

Fig. 4. The illustration for center of mass of a roly-poly toy. The upper part ($\mathcal{U}$) is the input mesh and the lower part ($\mathcal{L}$) is a paraboloid of revolution. (b) is an abstract model viewed from Y axis.

3.1.3. Inner filling

Based on the conclusions in Section 3.1.2, lower center of mass leads to better stability. We start our algorithm from filling the inner space of the 3D object. I stands for the filling pattern and I_U and I_L represent the filling pattern for $\mathcal{U}$ and $\mathcal{L}$, respectively.

The filling pattern for $\mathcal{U}$ is based on the method proposed by Prévost et al. (2013). They proposed the framework to manipulate mass distribution by alternating between interior carving (denoted as I_U) and shape deformation (denoted as T_U). As illustrated in Fig. 2 in Phase 1, such a method can change the position of center of mass from the original position C to the target position C' by carving the volume inside the candle while maintaining the outer surface.

It is obvious that filling $\mathcal{L}$ from the bottom to top will lower the center of mass of the toy with the same amount of printing material. Let C_M be the center of mass of the roly-poly toy, C_U and C_L the center of mass for $\mathcal{U}$ and $\mathcal{L}$, respectively. From Equation (3), it is easy to follow that the more material away from C_U, the lower C_M is.

3.2. Design issue

3.2.1. a, r constraint for $\mathcal{L}$

a controls the shape of the paraboloid and r determines the opening size of $\mathcal{L}$, which are key factors in regaining the balance for the roly-poly toy. We assume that the filling of $\mathcal{L}$ is from height 0 to height h as shown in Fig. 4(b). Then, r and h are related as following:

$$h = ar^2. \tag{9}$$

Let ρ be the density of the material, m_U the mass of $\mathcal{U}$, and m_L the mass of $\mathcal{L}$. We assume that points C_U and C_L are located at $(0, 0, c_U)$ and $(0, 0, c_L)$, respectively as shown in Fig. 4. Based on our filling strategy, $\mathcal{U}$ is placed on top of $\mathcal{L}$. Then the following equation stands:

$$c_U = c_U^0 + ar^2, \tag{10}$$

where c_U^0 is the height of the center of mass for $\mathcal{U}$ when we put $\mathcal{U}$ directly on the supporting plane. Thus, the mass m_L of $\mathcal{L}$ after the filling process is:

$$m_L = \rho \int_0^{ar^2} \frac{\pi}{a} z dz = \frac{1}{2} a \rho \pi r^4. \tag{11}$$

Based on the formula in Equation (3), C_L of $\mathcal{L}$ after the filling process can be calculated as:

$$c_L = \frac{1}{m_L} \rho \int_0^{ar^2} \frac{\pi}{a} z^2 dz = \frac{2}{3} ar^2. \tag{12}$$

Therefore, the position of C_M denoted as $(0, 0, c_M^z)$ is derived as:

$$c_M^z = \frac{c_U m_U + c_L m_L}{m_U + m_L} = \frac{c_U m_U + \frac{1}{3}\rho\pi a^2 r^6}{m_U + \frac{1}{2}\rho\pi a r^4}. \tag{13}$$

Considering Equation (8), the constraint for balancing is:

$$m_U + \frac{1}{2}\rho\pi a r^4 - 2ac_U m_U - \frac{2}{3}\rho\pi a^3 r^6 \geq 0. \tag{14}$$

If we only fabricate $\mathcal{L}$ as the roly-poly toy, Equation (14) can be further simplified into:

$$ar \leq \frac{\sqrt{3}}{2}. \tag{15}$$

3.2.2. Shape constraint

Interesting and adorable roly-poly toys require well designed shapes, which indicates that $\mathcal{L}$ is proportional to $\mathcal{U}$ considering its dimension. Therefore, we assume radius r_u of $\mathcal{U}$ matches with the radius r_L of $\mathcal{L}$. Thus, we adopt S to measure the shape constraint:

$$S = \frac{(r_u - r_l)^2}{{r_u}^2}. \tag{16}$$

When S decreases, a similar sized $\mathcal{L}$ is produced which makes the upper part be in harmony with the lower part.

3.2.3. Stability constraint

The stability to regain the initially balancing state is one of the key characters of roly-poly toys. We use P to describe the motion stability:

$$P = \frac{c_M^z}{\frac{1}{2a} + ar^2}, \tag{17}$$

which is derived from Equation (7). According to Equation (14), the value of P is between 0 to 1. The smaller the P is, the lower the center of mass is, and hence the more stable the roly-poly toy should be. A roly-poly toy with smaller P tends to regain balance by itself.

3.2.4. Swing amplitude constraint

The larger amplitude of swing is, the more interesting the roly-poly toy seems. We adopt D to represent the amplitude of swing:

$$D = \operatorname{arccot} 2ar. \tag{18}$$

As shown in Fig. 3(c), D is the cotangent of angle $\angle$BAE. Smaller D indicates a larger amplitude of swing. $\mathcal{L}$ is drawn as the connection of $OAED$. E is the intersect point of $\mathcal{L}$ and Y axis. Therefore,

$$AE = r,\ BO = \frac{1}{2a} + ar^2,\ EO = ar^2, \tag{19}$$

and

$$\angle \mathrm{ABE} = \angle \mathrm{EAH},\ \tan \angle \mathrm{ABE} = \frac{AE}{BE} = 2ar,\ \cot \angle \mathrm{BAE} = \frac{AE}{BE} = 2ar. \tag{20}$$

As $\angle$BAE decreases, $\angle$EAH increases. Thus, the designed toy gains a larger amplitude with smaller D.

3.3. Optimization

We aim to fabricate roly-poly toys with less time and less material while keeping upper parts and lower parts visually pleasant. Besides the basic constraint in Equation (3), the center of mass for $C_M = (c_M^x, c_M^y, c_M^z)$ should lie on the Z axis. Some parameters have direct impact on the fabricated results, such as the filling pattern I_U and I_L, the transformation of the upper part T_U, the posed position P_U of $\mathcal{U}$, and the coefficients a, r for determining the shape of $\mathcal{L}$. Thus, the optimization problem can be formulated as:

$$\begin{aligned} &\min_{a,r,I_U,I_L,T_U,P_U} \frac{m_M}{m_u} + \lambda_S S + \lambda_P P + \lambda_D D, \\ &\textbf{s.t.} \qquad c_M^x = 0, c_M^y = 0, c_M^z < \frac{1}{2a} \end{aligned} \tag{21}$$

where λ_S, λ_P, and λ_D are used to balance the weight between S, P, D.

The optimization for Equation (21) is nonlinear. To simplify the problem, we adopt several assumptions. We use the inner filling process to fill $\mathcal{L}$ to keep the balance, which sets a constant routine for I_L and have a direct influence on c_M^z. c_M^x and c_M^y are optimized by adjusting T_U and P_U. In order to speed up the process, we use an alternating optimization process to iteratively meet the constraints for c_M^x, c_M^y and c_M^z.

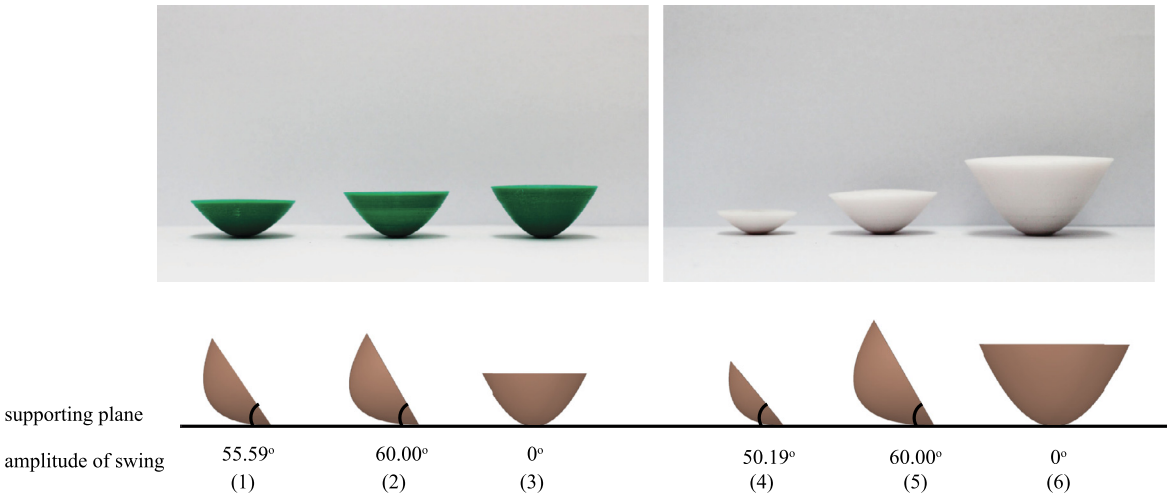

Fig. 5. The validation of Equation (15). The green ones labeled (1)–(3) are fabricated with same r and different a, while the white ones labeled (4)–(6) are fabricated with same a and different r. Details are shown in Table 1. They present different characteristics when pushed over. (For interpretation of the references to color in this figure legend, the reader is referred to the web version of this article.)

Table 1
Parameters for models in Fig. 5.

Model	a	r (mm)	ar	Satisfy the ar constraint	Amplitude
(1)	0.0292	25	0.7300	√	55.59^o
(2)	0.0346	25	0.8660	√	60.00^o
(3)	0.0400	25	1.0000	×	0^o
(4)	0.03	20	0.6000	√	50.19^o
(5)	0.03	28.86	0.8660	√	60^o
(6)	0.03	36	1.0800	×	0^o

In Phase 1, we set a, r unchanged and optimize parameters of $\mathcal{U}$ to satisfy the constraints for c_M^x, c_M^y:

$$\begin{aligned} &\min_{I_U, P_U, T_U} \quad m_U, \\ &\textbf{s.t.} \quad\quad c_M^x = 0, c_M^y = 0. \end{aligned} \tag{22}$$

Phase 1 is calculated based on the method by Prévost et al. (2013) to optimize I_U and T_U. However, several improvements are made. Prévost set the optimized target of center of mass at the rim of the safe region of the supporting region, while we set the target at the center of the supporting region instead for a visually pleasing shape. We also change selection of possible distribution of material to favor the solution with smaller mass. If the optimized target is not reached after the improved optimization of Prévost et al., the translation of $\mathcal{U}$ is adopted.

Phase 2 is optimized by ignoring the constraints for c_M^x, c_M^y and setting $\mathcal{U}$ unchanged. Equation (21) is set as:

$$\begin{aligned} &\min_{a,r} \quad \frac{\frac{1}{2}a\rho\pi r^4}{m_u} + \lambda_S \frac{(r_u - r_l)^2}{{r_u}^2} + \lambda_P \frac{c_M^z}{\frac{1}{2a} + ar^2} + \lambda_D \operatorname{arccot} 2ar, \\ &\textbf{s.t.} \quad m_U + \frac{1}{2}\rho\pi a r^4 - 2ac_U^0 m_U - 2a^2 r^2 m_U - \frac{2}{3}\rho\pi a^3 r^6 \geq 0. \end{aligned} \tag{23}$$

The optimization problem for Phase 2 is nonlinear and it is solved using genetic algorithm.

4. Results

We tested our method on a variety of examples. All the examples are printed using PLA plastic material with the fused decomposition modeling (FDM) technique. We set the parameters as follows: $\lambda_S = 0.2$, $\lambda_P = 0.2$, $\lambda_D = 6.0$.

Validation for the ar constraint in Equation (15). Without combining $\mathcal{U}$, the balancing condition of $\mathcal{L}$ is constrained to Equation (15). In Fig. 5, test results are printed on different values of a and r. The parameters are shown in Table 1. (2) and (5) reach the upper limit of Equation (15) and they have the largest amplitude of swing. As (3) and (6) fail to restore balancing by themselves, the amplitude is set to 0. (3) and (6) illustrate that with bigger $\mathcal{L}$ for the roly-poly toy is

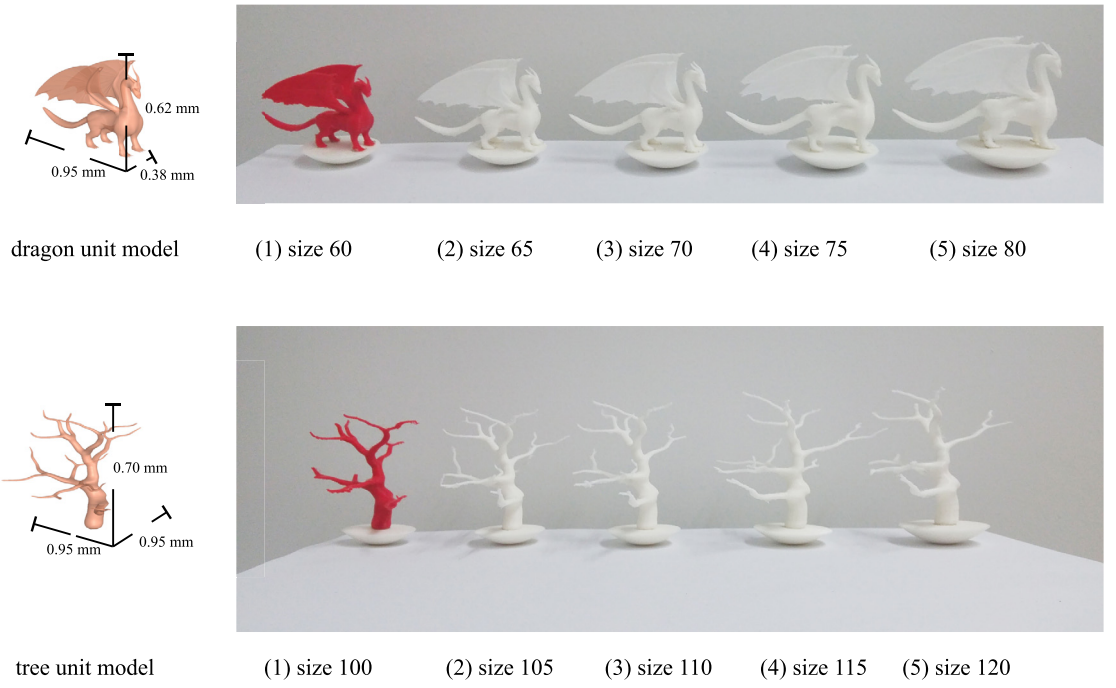

Fig. 6. Examples of dragons and trees.

Table 2
Optimization with different sizes of $\mathcal{U}$.

Model	Dragon					Tree				
	Size $\mathcal{U}$	a	r (mm)	ar	Amplitude	Size $\mathcal{U}$	a	r (mm)	ar	Amplitude
(1)	×60	0.0253	17.22	0.4357	41.07^o	×100	0.0205	20.97	0.43	40.70^o
(2)	×65	0.0234	18.74	0.4385	41.25^o	×105	0.0191	21.54	0.4120	39.49^o
(3)	×70	0.0219	20.31	0.4448	41.65^o	×110	0.0183	22.71	0.4157	39.74^o
(4)	×75	0.0204	21.75	0.4437	41.59^o	×115	0.0179	24.16	0.4325	40.86^o
(5)	×80	0.0194	24.12	0.4679	43.10^o	×120	0.0173	25.39	0.4392	41.30^o

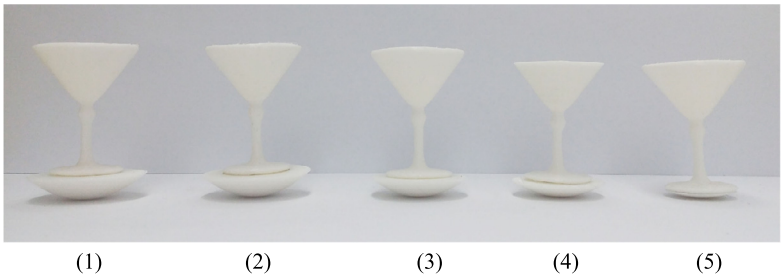

Fig. 7. Examples of goblets.

not always a good idea. If the parameters of a, r fail the ar constraint, $\mathcal{L}$ hardly balance themselves, which also proves that randomly selecting the shape of $\mathcal{L}$ to make a roly-poly toy is likely to fail.

Examples for $\mathcal{U}$ in different sizes. Fig. 6 shows the same model for $\mathcal{U}$ with different sizes. The dragon unit model is 0.95 mm in length × 0.38 mm in width × 0.62 mm in height as reference. The tree unit model is 0.95 mm in length × 0.95 mm in width × 0.70 mm in height. The details for model size and $\mathcal{L}$ are shown in Table 2. The size for printed model is compared to dragon and tree unit models respectively.

With different sizes, mass of the $\mathcal{U}$ and center of mass change correspondingly. The optimized $\mathcal{L}$ results vary consequently, which tends to have larger r and smaller a.

Comparisons with different weights for S. S is essential to the shape of a result, which affects the shape of combination of $\mathcal{U}$ and $\mathcal{L}$. The larger λ_S is, the better $\mathcal{U}$ and $\mathcal{L}$ match on the interface. For this goblet model example in Fig. 7,

Table 3
Optimization with different λ_S for goblet model.

Model	λ_S	a	r (mm)	ar	Amplitude
(1)	0	0.0224	20.59	0.4612	42.69^o
(2)	0.2	0.0212	19.36	0.4104	39.38^o
(3)	0.5	0.0207	18.85	0.3902	37.97^o
(4)	1.0	0.0193	17.39	0.3356	33.87^o
(5)	2.0	0.0164	12.50	0.2050	22.29^o

Fig. 8. Examples of girls. (a) is the balancing state. $\mathcal{U}$ use the same model. The white one is optimized using P and the red one is optimized without using P. The optimized results are $a = 0.0234$, $r = 25.7556$ for the left one and $a = 0.0237$, $r = 23.9305$ for the right one consequently. After pushing them in (a), the white one is more likely to regain its balancing state, while the red one is not, as shown in (b). (For interpretation of the references to color in this figure legend, the reader is referred to the web version of this article.)

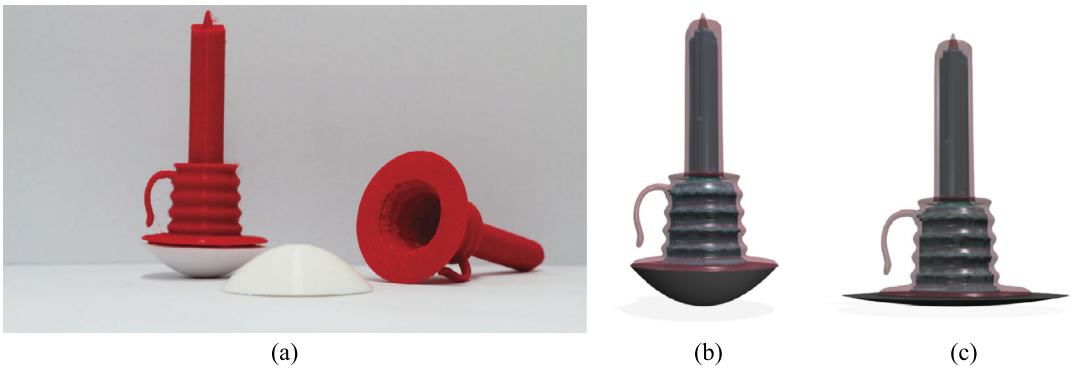

Fig. 9. Examples of candles. (a) shows the optimized results using our method. The mass and height of the upper part are 24.66 g and 95 mm, respectively, and that of the lower part are 5.79 g and 13.9 mm, respectively. With obvious difference in size and mass, the combination of the two parts is able to swing. (b) is our result and (c) is the result without using swing amplitude constraint (D). The outer surfaces are drawn pink in (b)–(c), while the inner surfaces are drawn in grey.

different results are produced with various λ_S as shown in Table 3. The radius (r_0) for $\mathcal{U}$ on the interface is 12.5 mm. With increasing λ_S, the optimized r for $\mathcal{L}$ tends to fit r_0. However, the amplitude decrease significantly.

Comparisons with and without P. P (Equation (17)) plays an essential part in the stability of the printed examples. Various deviations are introduced in the printing process including 3D printing process, removing the support material, combining $\mathcal{U}$ and $\mathcal{L}$ and so on. As shown in Fig. 8, these two roly-poly toys have the same $\mathcal{U}$. The left one is the result using our method and the right one is optimized with $\lambda_P = 0$. The optimized results for the left one ($a = 0.0234$, $r = 25.7556$) is slightly larger than the right one ($a = 0.0237$, $r = 23.9305$). The left one is more likely to regain its balancing state when pushed over.

Comparisons with and without D. D affects the amplitude of swing for the roly-poly toy. Fig. 9 is an example of optimized results with and without D.

The $\mathcal{U}$ is hollowed inside. (b) is our result with $a = 0.0209$, $r = 25.80$, while (c) ($a = 0.0025$, $r = 37.55$) is optimized with $\lambda_D = 0$. The comparison results are straightforward. With the $\mathcal{L}$ produced in (c), the roly-poly toy is sufficiently stable. However, the swing amplitude is limited.

Fig. 10. More results.

5. Conclusions and discussions

We have introduced an effective method to design personalized roly-poly toys. Our optimized toys can regain balance by themselves when they are pushed over. We also favor a well-balanced shape and a larger amplitude of swing without reducing the motion stability. The effectiveness of our method are validated by various results. (See Fig. 10.)

Our method has some limitations. (1). The center of mass position of $\mathcal{U}$ in Phase 1 is adjusted through inner carving, which may limit the shape of the resulting toy. One solution to eliminate this limitation is to optimize the shape of $\mathcal{U}$ (Hu et al., 2015). (2). We use the same material for both $\mathcal{U}$ and $\mathcal{L}$. Employing multiple materials will enable the optimization process with more degrees of freedom and produce more visually pleasing results. For example, we can use a larger density material for $\mathcal{L}$ and a lighter density material for $\mathcal{U}$ to increase the stability of the resulting toy. (3). The upper part and the base are optimized separately. It will be interesting to merge $\mathcal{U}$ and $\mathcal{L}$ first and then optimize the whole merged shape directly. We will leave it as our future work.

Acknowledgements

We would like to thank the anonymous reviewers for their valuable suggestions. Juncong Lin is supported in part by grants from the National Natural Science Foundation of China (No. 61202142) and the National Key Technology R&D Program Foundation of China (No. 2015BAH16F00/F02). Xiaogang Jin is supported by the National Natural Science Foundation of China (No. 61472351). Weiwei Xu is partially supported by the National Natural Science Foundation of China (No. 61322204).

Appendix A. Supplementary material

Supplementary material related to this article can be found online at http://dx.doi.org/10.1016/j.cagd.2016.02.001.

References

Bächer, M., Bickel, B., James, D.L., Pfister, H., 2012. Fabricating articulated characters from skinned meshes. ACM Trans. Graph. 31 (4), 47. http://dx.doi.org/10.1145/2185520.2185543.

Bächer, M., Whiting, E., Bickel, B., Sorkine-Hornung, O., 2014. Spin-it: optimizing moment of inertia for spinnable objects. ACM Trans. Graph. 33 (4), 96. http://dx.doi.org/10.1145/2601097.2601157.

Bickel, B., Bächer, M., Otaduy, M.A., Lee, H.R., Pfister, H., Gross, M., Matusik, W., 2010. Design and fabrication of materials with desired deformation behavior. ACM Trans. Graph. 29 (4), 63. http://dx.doi.org/10.1145/1778765.1778800.

Calì, J., Calian, D.A., Amati, C., Kleinberger, R., Steed, A., Kautz, J., Weyrich, T., 2012. 3D-printing of non-assembly, articulated models. ACM Trans. Graph. 31 (6), 130. http://dx.doi.org/10.1145/2366145.2366149.

Ceylan, D., Li, W., Mitra, N.J., Agrawala, M., Pauly, M., 2013. Designing and fabricating mechanical automata from mocap sequences. ACM Trans. Graph. 32 (6), 186. http://dx.doi.org/10.1145/2508363.2508400.

Chen, D., Levin, D.I.W., Didyk, P., Sitthi-Amorn, P., Matusik, W., 2013. Spec2Fab: a reducer-tuner model for translating specifications to 3D prints. ACM Trans. Graph. 32 (4), 135. http://dx.doi.org/10.1145/2461912.2461994.

Chen, X., Zheng, C., Xu, W., Zhou, K., 2014. An asymptotic numerical method for inverse elastic shape design. ACM Trans. Graph. 33 (4), 95. http://dx.doi.org/10.1145/2601097.2601189.

Coros, S., Thomaszewski, B., Noris, G., Sueda, S., Forberg, M., Sumner, R.W., Matusik, W., Bickel, B., 2013. Computational design of mechanical characters. ACM Trans. Graph. 32 (4), 83. http://dx.doi.org/10.1145/2461912.2461953.

Deuss, M., Panozzo, D., Whiting, E., Liu, Y., Block, P., Sorkine-Hornung, O., Pauly, M., 2014. Assembling self-supporting structures. ACM Trans. Graph. 33 (6), 214. http://dx.doi.org/10.1145/2661229.2661266.

Eberly, D.H., 2010. Game Physics. Taylor and Francis.

Guo, X., Lin, J., Xu, K., Jin, X., 2014. Creature grammar for creative modeling of 3D monsters. In: Geometric Modeling and Processing 2014. Graph. Models 76 (5), 376–389. http://dx.doi.org/10.1016/j.gmod.2014.03.019.

Halliday, D., Resnick, R., Krane, K.S., 1992. Physics. Vol. 1. Wiley.

Hirose, M., Mitani, J., Kanamori, Y., Fukui, Y., 2011. An interactive design system for sphericon-based geometric toys using conical voxels. In: Proceedings of the 11th International Conference on Smart Graphics. SG'11. Springer-Verlag, Berlin, Heidelberg, pp. 37–47.

Hu, K., Jin, S., Wang, C.C., 2015. Support slimming for single material based additive manufacturing. Comput. Aided Des. 65, 1–10. http://dx.doi.org/10.1016/j.cad.2015.03.001.

Igarashi, Y., Igarashi, T., 2009. Designing plush toys with a computer. Commun. ACM 52 (12), 81–88. http://dx.doi.org/10.1145/1610252.1610275.

krokotak.com, 2015. The egg that never falls. http://krokotak.com/2013/04/the-egg-that-never-falls/.

Kwok, T.H., Wang, C.C.L., Deng, D., Zhang, Y., Chen, Y., 2015. 4D printing for freeform surfaces: design optimization of origami and kirigami structures. ASME Transactions. In: Special Issue on Design for Additive Manufacturing. J. Mech. Des. 137 (11). http://dx.doi.org/10.1115/1.4031023.

Kyburz, J.A., 1994. "Omocha": things to play (or not to play) with. Asian Folk. Stud. 53 (1), 1–28. http://dx.doi.org/10.2307/1178558.

Lan, Y., Dong, Y., Pellacini, F., Tong, X., 2013. Bi-scale appearance fabrication. ACM Trans. Graph. 32 (4), 145. http://dx.doi.org/10.1145/2461912.2461989.

Liu, S., Wang, C.C., 2011. Fast intersection-free offset surface generation from freeform models with triangular meshes. IEEE Trans. Autom. Sci. Eng. 8 (2), 347–360. http://dx.doi.org/10.1109/TASE.2010.2066563.

Lo, K.-Y., Fu, C.-W., Li, H., 2009. 3D polyomino puzzle. In: ACM SIGGRAPH Asia 2009 Papers. SIGGRAPH Asia '09. ACM, New York, NY, USA, 157.

Luo, S.-J., Yue, Y., Huang, C.-K., Chung, Y.-H., Imai, S., Nishita, T., Chen, B.-Y., 2015. Legolization: optimizing lego designs. ACM Trans. Graph. 34 (6), 222:1–222:12. http://dx.doi.org/10.1145/2816795.2818091.

Mitani, J., Suzuki, H., 2004. Making papercraft toys from meshes using strip-based approximate unfolding. In: ACM SIGGRAPH 2004 Papers. SIGGRAPH '04. ACM, New York, NY, USA, pp. 259–263.

Mori, Y., Igarashi, T., 2007. Plushie: an interactive design system for plush toys. ACM Trans. Graph. 26 (3). http://dx.doi.org/10.1145/1276377.1276433.

Mueller, S., Mohr, T., Guenther, K., Frohnhofen, J., Rollmann, K.-A., Baudisch, P., 2014. faBrickation: fast 3D printing of functional objects by integrating construction kit building blocks. In: CHI '14 Extended Abstracts on Human Factors in Computing Systems. CHI EA '14. ACM, New York, NY, USA, pp. 527–530.

Musialski, P., Auzinger, T., Birsak, M., Wimmer, M., Kobbelt, L., 2015. Reduced-order shape optimization using offset surfaces. ACM Trans. Graph. 34 (4), 102. http://dx.doi.org/10.1145/2766955.

Panozzo, D., Block, P., Sorkine-Hornung, O., 2013. Designing unreinforced masonry models. ACM Trans. Graph. 32 (4), 91. http://dx.doi.org/10.1145/2461912.2461958.

Perelman, G., Serrano, M., Raynal, M., Picard, C., Derras, M., Dubois, E., 2015. The roly-poly mouse: designing a rolling input device unifying 2D and 3D interaction. In: Proceedings of the 33rd Annual ACM Conference on Human Factors in Computing Systems. CHI '15. ACM, New York, NY, USA, pp. 327–336.

Prévost, R., Whiting, E., Lefebvre, S., Sorkine-Hornung, O., 2013. Make it stand: balancing shapes for 3D fabrication. ACM Trans. Graph. 32 (4), 81. http://dx.doi.org/10.1145/2461912.2461957.

Song, P., Fu, C.-W., Cohen-Or, D., 2012. Recursive interlocking puzzles. ACM Trans. Graph. 31 (6), 128. http://dx.doi.org/10.1145/2366145.2366147.

Stava, O., Vanek, J., Benes, B., Carr, N., Měch, R., 2012. Stress relief: improving structural strength of 3D printable objects. ACM Trans. Graph. 31 (4), 48. http://dx.doi.org/10.1145/2185520.2185544.

vigothecarpathian, 2015. Make your own egg weeble wobble toys. http://www.instructables.com/id/Make-your-own-Egg-Weeble-Wobble-Toys/.

Wang, C.C., Manocha, D., 2013. GPU-based offset surface computation using point samples. In: Solid and Physical Modeling 2012. Comput. Aided Des. 45 (2), 321–330. http://dx.doi.org/10.1016/j.cad.2012.10.015.

Whiting, E., Ochsendorf, J., Durand, F., 2009. Procedural modeling of structurally-sound masonry buildings. ACM Trans. Graph. 28 (5), 112. http://dx.doi.org/10.1145/1618452.1618458.

Whiting, E., Shin, H., Wang, R., Ochsendorf, J., Durand, F., 2012. Structural optimization of 3D masonry buildings. ACM Trans. Graph. 31 (6), 159. http://dx.doi.org/10.1145/2366145.2366178.

Wikipedia, 2016. Roly-poly toy — Wikipedia, the free encyclopedia. https://en.wikipedia.org/wiki/Roly-poly_toy.

Xin, S., Lai, C.-F., Fu, C.-W., Wong, T.-T., He, Y., Cohen-Or, D., 2011. Making burr puzzles from 3D models. In: ACM SIGGRAPH 2011 Papers. SIGGRAPH '11. ACM, New York, NY, USA, 97.

Zhang, X., Le, X., Panotopoulou, A., Whiting, E., Wang, C.C.L., 2015. Perceptual models of preference in 3D printing direction. ACM Trans. Graph. 34 (6), 215. http://dx.doi.org/10.1145/2816795.2818121.

Zhou, Q., Panetta, J., Zorin, D., 2013. Worst-case structural analysis. ACM Trans. Graph. 32 (4), 137. http://dx.doi.org/10.1145/2461912.2461967.

Zhu, L., Xu, W., Snyder, J., Liu, Y., Wang, G., Guo, B., 2012. Motion-guided mechanical toy modeling. ACM Trans. Graph. 31 (6), 127. http://dx.doi.org/10.1145/2366145.2366146.